The Japan Society of Mechanical Engineers

Output Characteristics of a Thin-Film Piezoelectric AE Sensor for Magnetic Head-Disk Interaction*

Satomitsu IMAI**, G. J. BURGER***,
T. S. J. LAMMERINK*** and J. H. J. FLUITMAN***

A new type of acoustic emission (AE) sensor was developed for detecting head-disk interaction in magnetic disk devices. In order to develop a small sensor, we used a thin-film piezoelectric material and mounted it on the Si slider using micromachining techniques. We conducted a basic experiment and a simulation of sensor output, and confirmed that the simulation used here can predict sensor output characteristics. This paper describes the structure of the sensor and the method of simulation. We also performed several other simulations of sensor output characteristics using this method, and confirmed that the new sensor is applicable to tribological research on head-disk interaction.

Key Words: Sensor, Piezoelement, Impact, Acoustic Emission, Sensitivity Analysis, Tribology, Magnetic Disk, Micromachine

1. Introduction

Flying height of sliders in magnetic disk systems has been decreasing in order to increase recording density and it is around 50 nm at present. Accurate measurement of the contact between the slider and the disk surface is becoming increasingly important in evaluating the head-disk interface. As a conventional method, a bulk piezoelectric material has been used as an acoustic emission (AE) sensor by gluing it to the back of a slider. However, greater compactness and accuracy are required for AE sensors for the downsizing of sliders and the study of the microtribology of the head-disk interface.

Therefore, we developed a new AE sensor using a thin-film piezoelectric material embedded in the slider, using micromachine techniques[1],[2] and conducted a fundamental output test of the sensor. We contrived a method for simulating the output of the sensor and confirmed its validity by comparing the result of the simulation with that of the sensor output test. Furthermore, we examined other output characteristics of the sensor by this simulation method.

* Recieved 19th June, 1996. Japanese original: Trans. Jpn. Soc. Mech. Eng., Vol. 62, No. 595, C (1996), pp. 928-935 (Recieved 26th June, 1995)
** Data Storage and Retrieval Systems Division, Hitachi, Ltd., 2880 Kozu, Odawara, Kanagawa 256, Japan
*** MESA Research Institute, University of Twente, 7500 AE Enschede, the Netherlands

2. Structure of the Thin-Film AE Sensor and the Slider

2.1 Structure of the thin-film AE sensor

Figure 1 shows the structure of the thin-film AE sensor. The sensor has a sputtered zinc oxide (ZnO) piezoelectric layer (thickness: 2 μm) sandwiched by

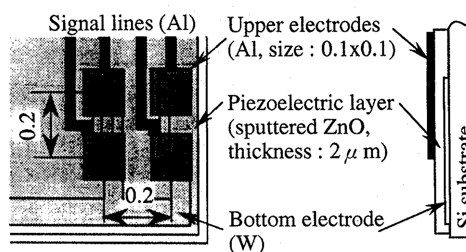

Fig. 1 Structure of the thin-film piezoelectric AE sensor array

NII-Electronic Library Service

The Japan Society of Mechanical Engineers

the upper arrayed electrodes and lower common electrode formed by electron beam deposition. The dielectric direction (c-axis) is perpendicular to the Si substrate. The sensor is arrayed to enable the examination of the relation between sensor output and sensor position. The area of each upper electrode is 0.1 mm×0.1 mm.

2.2 Structure of the slider

Figure 2 shows the structure of the sensor slider. The slider is composed of a Si substrate mounted with the sensor, where the backing material acts as an acoustic matching layer of the sensor. The backing material prevents AE waves from reflecting off the back of the sensor which decreases the S/N ratio of the sensor. We chose Pyrex glass as the backing material, since its acoustic impedance is close to that of the Si substrate. The air bearing surface (ABS) of the slider is fabricated on the surface of the Si substrate opposite the sensor. The AE waves due to contact propagate from the ABS to the sensor through the Si substrate. The ABS is a conventional 2 rail type and has front steps in the leading edge of the rails, instead of the tapers found in conventional sliders[3].

The slider is 3 mm long and 2.4 mm wide (70% slider). The thickness of the Si substrate is 0.38 mm, the thickness of the Pyrex glass is 0.5 mm, and the total thickness of the slider is about 0.88 mm. The sensor is located in the trailing edge of the outer rail at which the flying height of the slider is minimum. Signals of the sensor are obtained from the bonding pads on the slider.

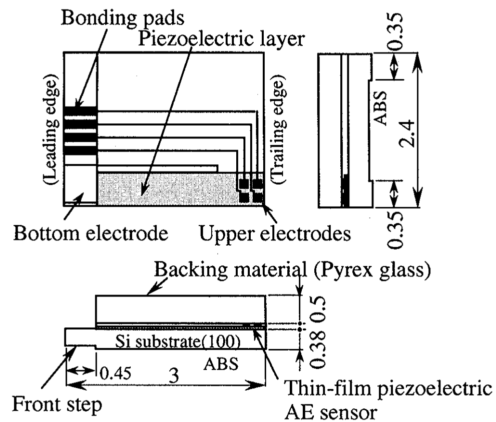

Fig. 2 Structure of the slider carrying the thin-film piezoelectric sensor array (Depth of the ABS slot is 20 μm.)

3. Simulation of Sensor Output

3.1 Simulation method

Figure 3 shows a physical model of the AE sensor shown in Fig. 2. The piezoelectric layer (p) of the sensor is modeled as a 3-port system: port 1 is the acoustic input port of AE waves from the Si substrate (a), port 2 is the acoustic output port of AE waves to the backing material (b) and port 3 is the electric output port of the voltage in the form of the AE waves through the sensor. The AE wave is considered as a plane wave here.

We define that at the acoustic input and output ports 1 and 2, the force due to the AE wave is $F_n(n=1, 2)$, the velocity of AE wave is $v_n(n=1, 2)$, and the acoustic impedances of the Si substrate, the backing material and the piezoelectric layer are Z_{0a}, Z_{0b} and Z_{0p} respectively. The electric impedance of the piezoelectric layer is Z_e. The area and the thickness of the piezoelectric layer are t_p and A. The densities of the Si substrate, the backing material and the piezoelectric material are ρ_a, ρ_b, and ρ_p prespectively.

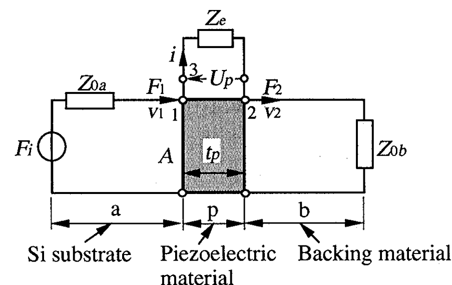

Fig. 3 Physical model of the thin-film AE sensor and slider

The equilibrium equations at those 3 ports are[4]

$$F_1=F_i-v_1Z_{0a} \tag{1}$$

$$F_2=v_2Z_{0b} \tag{2}$$

$$u_p=-iZ_e \tag{3}$$

$$\begin{bmatrix} F_1 \\ F_2 \\ u_p \end{bmatrix} = -jZ_{0p}\begin{bmatrix} \cot(k_p t_p) & -\csc(k_p t_p) & h_{33}/\omega Z_{0p} \\ \csc(k_p t_p) & -\cot(k_p t_p) & h_{33}/\omega Z_{0p} \\ h_{33}/\omega Z_{0p} & -h_{33}/\omega Z_{0p} & 1/\omega C_0 Z_{0p} \end{bmatrix} \times \begin{bmatrix} v_1 \\ v_2 \\ i \end{bmatrix} \tag{4}$$

where

$$\left.\begin{aligned} Z_{0a}&=A\sqrt{\rho_a/s_{33a}} \\ Z_{0b}&=A\sqrt{\rho_b/s_{33b}} \\ Z_{0p}&=A\sqrt{\rho_p/s_{33p}^D} \end{aligned}\right\} \tag{5}$$

$$k_p=\omega\sqrt{\rho_p s_{33p}^D} \tag{6}$$

(k_p: wave number, ω: angular frequency, s_{33}: elastic compliance)

$$C_0=\varepsilon_{33}^S A/t_p \tag{7}$$

Subscript 33 means the thickness direction.

d_{33}: piezoelectric constant (strain by unit electric field)

h_{33}: piezoelectric constant (electric field by unit strain)

$$h_{33}=-d_{33}/(\varepsilon_{33}^T\ s_{33}^E-d_{33}^2) \tag{8}$$

ε_{33}^S: dielectric constant (at constant strain)

NII-Electronic Library Service

The Japan Society of Mechanical Engineers

Table 1 Material properties

Material	Density ρ kg/m^3	Young's modulus E x10^{11}Pa	Poisson's ratio ν	Wave velocity c m/s (*3)	Acoustic impedance $Z0$ x10^7 Ns/m^3 (*4)
Si (100)	2332	1.302	0.28	8449	1.970
ZnO	5720	1.951	0.3	6775	3.875
Pyrex glass	7650	1.111	0.25	4175	3.194
PZT(*1)	7550	1.075	0.328	4576	3.455
$Al_2O_3 \cdot TiC$(*2)	4270	4.50	0.3	11911	5.086

(*1) Zr / Ti = 50 / 50
(*2) Al_2O_3 / TiC = 65 / 35
(*3) $c=\sqrt{(1-\nu)E/((1+\nu)(1-2\nu)\rho)}$ (5)
(*4) $Z_0=\rho c$

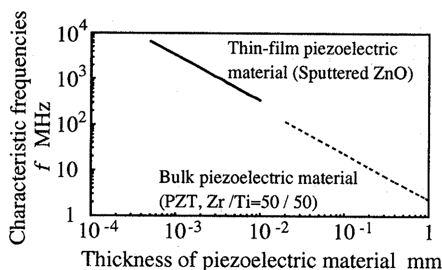

Fig. 4 Characteristic frequencies of piezoelectric materials in the thickness directions ($f=c/(2t_p)$, c: wave velocity, see Table 1)

ε^T_{33} : dielectric constant (at no constraint of strain)

s^D_{33p} : compliance (at constant electric field)

s^E_{33p} : elastic compliance (at no constraint of electric field)

Figure 4 shows the relation between the thickness of the piezoelectric layer and the natural frequency in the thickness direction, which is calculated from the velocities of AE waves shown in Table 1. Since the bandwidth of the AE waves measured is much less than the natural frequency of the piezoelectric layer in the thickness of 2 μm, $k_p t_p$ in Eq. (4) is approximately zero. Also, we can assume $F_1=F_2=F$ because the piezoelectric layer is thin. Therefore, Eq. (4) becomes

$$\begin{bmatrix} F \\ u_p \end{bmatrix} = \begin{bmatrix} \dfrac{1}{j\omega C_m} & \dfrac{h_{33}}{j\omega} \\ \dfrac{h_{33}}{j\omega} & \dfrac{1}{j\omega C_0} \end{bmatrix} \begin{bmatrix} v_1-v_2 \\ i \end{bmatrix} \tag{9}$$

where

$$C_m=s^D_{33}t_p/A \tag{10}$$

From the set of Eqs. (1)-(3), and (9), the voltage in the piezoelectric layer can be solved as follows.

$$u_p=\frac{d_{33}t_p}{A\varepsilon^T_{33}}\frac{Z_{0b}}{Z_{0a}+Z_{0b}}F_i \tag{11}$$

From Eq. (11), the electric capacitance of the sensor electrode can be expressed as follows.

$$C_p=\frac{A\varepsilon^T_{33}}{t_p} \tag{12}$$

When we measure the sensor output voltage (u_p), the parasitic capacitance of the measuring system reduces the output of the sensor. The sensor output measured (u_0) is expressed using Eq. (13) ($u_0<u_p$) on the basis of Fig. 5 which shows the equivalent electric circuit of the sensor and the measuring system, in which C_p is the electric capacitance of the sensor electrode, C_e is the parasitic capacitance of the measuring system, and R_e is the input resistance of the measuring system.

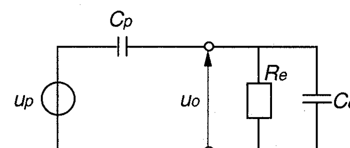

Fig. 5 Electric model of a measuring system

$$u_0=u_p\frac{j\omega R_e C_p}{(1+j\omega R_e(C_p+C_e))} \tag{13}$$

Since ω in Eq. (13) is quite high ($1 \ll j\omega R_e(C_p+C_e)$), Eq. (13) becomes as follows.

$$\begin{aligned} u_0 &= u_p C_p/(C_p+C_e) \\ &= F_i\frac{d_{33}t_p}{A\varepsilon^T_{33}}\frac{Z_{0b}}{Z_{0a}+Z_{0b}}\frac{C_p}{C_p+C_e} \end{aligned} \tag{14}$$

Equation (14) is expressed as follows in terms of the stress (σ_z) of the piezoelectric layer in the thickness direction ($\sigma_z<0$: compression, $\sigma_z>0$: tension).

$$\begin{aligned} u_0 &= -\sigma_z\frac{d_{33}t_p}{\varepsilon^T_{33}}\frac{C_p}{C_p+C_e} \\ &= -\sigma_z d_{33}A\frac{1}{\dfrac{A\varepsilon^T_{33}}{t_p}+C_e} \end{aligned} \tag{15}$$

In Eq. (15), we can see that output of the sensor depends on the stress (σ_z) of the piezoelectric layer and the capacitance (C_p) of the sensor. The stress is determined by factors such as the sensor structure, area (A), thickness (t_p), and sensor position. The capacitance is determined from the sensor area and the thickness of the piezoelectric layer, as shown in Eq. (12). Among the above factors, the area and the thickness of the sensor are related to both the stress and the capacitance of the sensor. Therefore, it is important to optimize these design parameters to get high sensitivity of the sensor.

NII-Electronic Library Service

The Japan Society of Mechanical Engineers

3. 2 Check of reliability of the simulation method

3. 2. 1 Sensor output for a dropped ball We measured output of the sensor for the input of the impact force of a dropped ball. The slider was fixed to the back of the backing material, as shown in Fig. 6, and a steel ball of 1 mm in diameter was dropped onto the center of one of the sensor elements from the height of 20 mm. The maximum input force of the dropped ball (F_{max}), the impact duration (T) and the time function of the impact force ($f(t)$) can be determined using the following equations[6]. Table 2 shows the properties of materials used in this test.

$$F_{max}=\pi a^2 P_{max} \quad (16)$$
$$a=1.31\rho^{0.2}k^{0.2}rv^{0.4}$$
$$k=(1-\nu_1^2)/E_1+(1-\nu_2^2)/E_2$$
$$P_{max}=0.558\rho^{0.2}v^{0.4}k^{-0.8}$$
$$T=5.08r\rho^{0.4}k^{0.4}v^{-0.2} \quad (17)$$
$$f(t)=F_{max}\sin^{1.63}(\pi t/T) \quad (18)$$

The maximum value of the input force is 1.88 N and the impact duration is 4.94 μs, on the basis of Eqs. (16) and (17). Figure 6 shows the output signal of the sensor. The maximum voltage of the output signal is 84 mV (amplified×6.25) and the sensitivity of the sensor is 7.1 mV/N. The impact duration calculated using Eq. (17) is almost the same as that of the experiment.

3. 2. 2 Simulation of the sensor output in the experiment We simulated sensor output in the ball drop test by the simulation method described in section 3. 1 and examined its validity. We calculated the stress of the piezoelectric layer in the thickness direction (σ_z) in Eq. (15) by a finite-element method (FEM). Figure 7 shows the finite-element model of the sensor slider. To simulate the FEM, we used DYNA 3 D (Lawrence Livermore National Laboratory, USA). The time function of the impact force calculated by Eq. (18) is the input in the FEM. Tables 1 and 3 show the constants in this simulation. The capacitance of the sensor element (C_p) in Eq. (15) is 0.365 pF from Eq. (12) and the parasitic capacitance of the measuring circuit (C_e) is 63 pF by measurement.

Figure 8 shows the simulated sensor output. Comparing it with the result of the experiment shown in Fig. 6, we can see that the maximum output of the sensor in the experiment (84 mV) is less than that in the simulation (137 mV). The reason might be that in the experiment the adhesive layer between the sensor and the backing material decreased the stress caused in the piezoelectric layer.

We conducted a sensor output simulation by calculating the stress of the piezoelectric layer using Eq. (19) which expresses the stress in a semi-infinite plate as a static force on the surface[7]. The average stress of the piezoelectric layer is obtained by surface integration of Eq. (19) in the sensor area ($r=-0.05 \sim +0.05$ mm, $z=0.38$ mm) in Fig. 9, as shown by Eq. (20). Figure 8 shows the sensor output by this stress calculation. In this case, the maximum sensor output (36.7 mV) is less than that of the experiment because the input force is static in this case.

Table 2 Material properties

ρ	Mass density of the ball kg/m^3	7.78 x10^3
r	Radius of the ball m	0.0005
v	Velocity of the ball before impact m/s	0.626
E_1	Young's modulus of the ball Pa	2.06 x10^{11}
ν_1	Poisson's ratio of the ball	0.3
E_2	Young's modulus of the ABS protection layer (SiO_2) Pa	0.724 x10^{11}
ν_2	Poisson's ratio of the ABS protection layer (SiO_2)	0.26

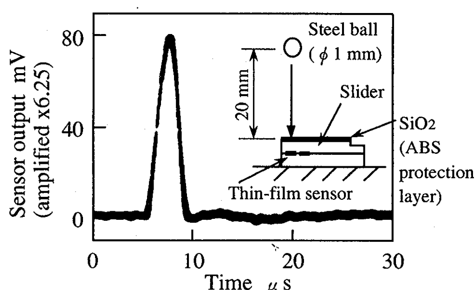

Fig. 6 Sensor output signal by the ball drop test
Specifications of the amplifier
amplification factor: ×6.25; bandwidth: 10 Hz-20 MHz; parasitic capacitance: 3 pF

Table 3 Piezoelectric constants

Properties			ZnO(*1)	PZT(*2)
ε_{33}^T	X10^{-9}	F/m	0.073	7.491
ε_{33}^S	X10^{-9}	F/m	0.053	5.240
d_{33}	X10^{-12}	C/N	12.3	173
h_{33}	X10^{10}	N/C	-3.29	-0.248
s_{33}^E	X10^{-12}	m^2/N (*3)	7.20	13.3
s_{33}^D	X10^{-12}	m^2/N	5.13	9.304
ρ		kg/m^3	5720	7550

(*1) : Sputtered ZnO
(*2) : Zr / Ti = 50 / 50 [5]
(*3) : S_{33}^D is used in the stress calculations of the piezoelectric materials.

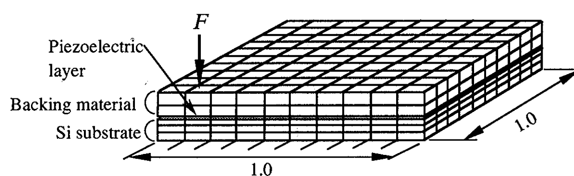

Fig. 7 Finite element model for the simulation of the sensor output test

NII-Electronic Library Service

The Japan Society of Mechanical Engineers

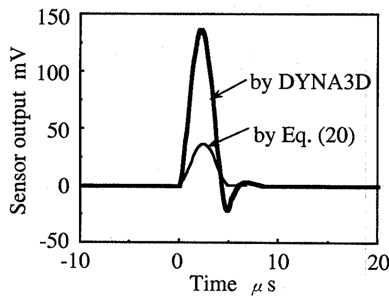

Fig. 8 Simulation of the sensor output test
Stress of the ZnO layer was calculated by DYNA 3 D and Eq. (20)
Simulation parameters. Sensor size: 0.1 mm × 0.1 mm; thickness: Si substrate 0.38 mm, ZnO layer 0.002 mm, backing material 0.5 mm; F=1.88 N; C_p=0.365 pF; C_e=63 pF; material properties: Tables 1 and 3

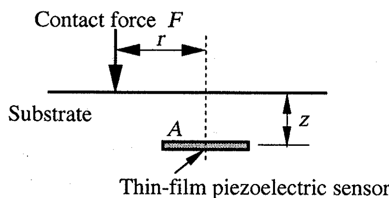

Fig. 9 Definition of position of the thin-film piezoelectric sensor

Comparing the sensor output simulated using the two methods of stress calculation with the result of the experiment, we believe that the simulated results are reasonable and the simulation method in section 3.1 is applicable.

$$\sigma_z=-\frac{3F}{2\pi}z^3(r^2+z^2)^{-2/5} \quad (19)$$

$$\overline{\sigma_z}=1/A\int_A \sigma_z dA \quad (20)$$

4. Simulation of Output Characteristics of the Sensor

We examined output characteristics of the sensor by the simulation method described in section 3.1. Because stress in the slider is complicated by reflections of AE waves on the boundary surfaces between different materials, we used a finite-element analysis (DYNA 3 D) to calculate stress (σ_z) of the piezoelectric layer of the sensor. Figure 10 shows a cross section of the finite-element model of the sensor slider. Fig. 10 shows (a) the model of the slider with the thin-film sensor and (b) the slider with a conventional sensor. The conventional sensor slider is used for comparing its output with that of the thin-film sensor. Since the AE waves propagate in the slider thickness direction, the finite-element models are simplified in the lateral directions of the sliders.

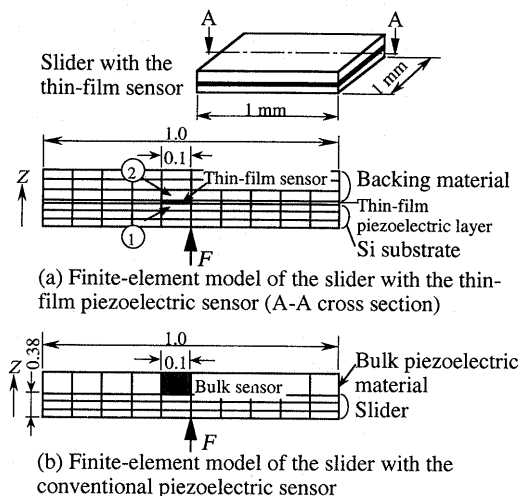

Fig. 10 Finite-element models for stress calculation

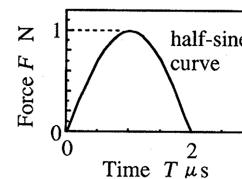

Fig. 11 Input force for the simulations

The size of each sensor is 0.1 mm × 0.1 mm. The constraint condition of the finite-element models is free under the flying condition. The input force is assumed to exhibit the half-sine curve shown in Fig. 11. The constants in the simulation are shown in Tables 1 and 3. The duration of the input force is 2 μs, which is in a normal range of the contact duration in measurement. We assume the parasitic capacitance C_e in Eq. (15) to be 60 pF on the basis of the discussion in section 3.2.

4.1 Output characteristics of the thin-film sensor and a conventional sensor

We compare output characteristics of the thin-film sensor and a conventional bulk sensor. In the simulation, the slider material of a conventional sensor is alumina-titanium-carbide ($Al_2O_3 \cdot TiC$) and the material of a conventional sensor is PZT ($PbZrO_3 \cdot PbTiO_3$). The thickness of the slider is 0.38 mm and the thickness of the sensor is a parameter.

Figure 12 shows the simulated relation between the thickness of the conventional sensor and the maximum output of the sensor. The maximum output increases as the thickness becomes large. This may be because the conventional sensor is considered to be a mechanical system comprised of the sensor's mass and a spring which corresponds to the stiffness of the sensor, and a thicker sensor causes greater inertia, which increases the sensor's output.

Figure 13 shows the simulated relation between

NII-Electronic Library Service

The Japan Society of Mechanical Engineers

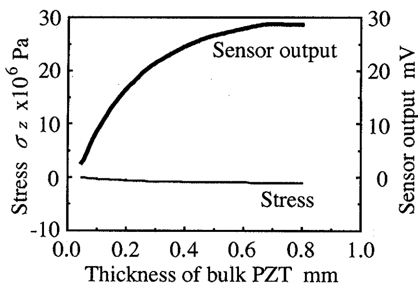

Fig. 12 Simulation of the maximum stress and the maximum sensor output of the conventional AE sensor
Simulation conditions
input force: Fig. 11; sensor size: 0.1 mm×0.1 mm; thickness: slider (Al_2O_3·TiC) 0.38 mm; C_p: from Eq. (12); C_e=60 pF; stress calculation: by DYNA 3 D

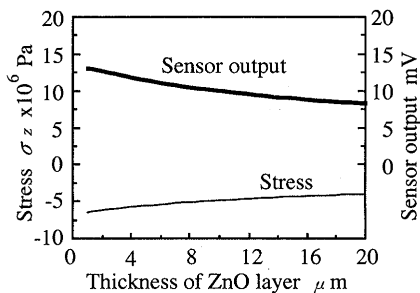

Fig. 13 Simulation of the maximum stress and the maximum sensor output of the thin-film piezoelectric AE sensor
Simulation conditions
input force: Fig. 11; sensor size: 0.1 mm×0.1 mm; thickness: Si substrate 0.38 mm, backing material 0.5 mm; C_p: from Eq. (12); C_e=60 pF; stress calculation: by DYNA 3 D

the thickness of the piezoelectric layer of the thin-film sensor and the maximum sensor output. The maximum sensor output decreases as the thickness of the piezoelectric layer increases. This characteristic is different from that of the conventional sensor. The reason may be that since the sensor is fabricated inside the slider, the stress of the piezoelectric layer becomes small as the distance between the input force and the sensor becomes large. Therefore, the average stress of the piezoelectric layer becomes small when the thickness of the piezoelectric layer is large.

From the simulated results, the maximum output of the conventional sensor by unit input force is 26.6 mV/N, while that of the thin-film sensor is 12.6 mV/N. The maximum output of the thin-film sensor is about half that of the conventional sensor. The difference in the maximum output of the two sensors is not as great as that in the sensor size.

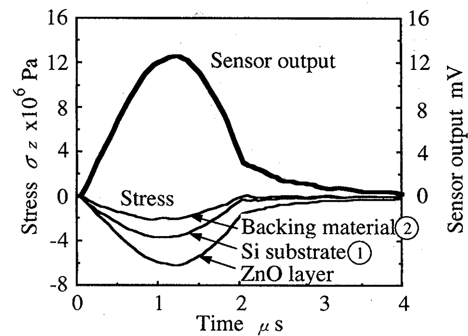

Fig. 14 Simulation of stress and sensor output of the thin-film piezoelectric AE sensor (with backing material)
Simulation conditions
input force: Fig. 11; sensor size: 0.1 mm×0.1 mm; thickness: Si substrate 0.38 mm, ZnO layer 0.002 mm, backing material 0.5 mm; C_p=0.365 pF; C_e=60 pF; stress calculation: by DYNA 3 D

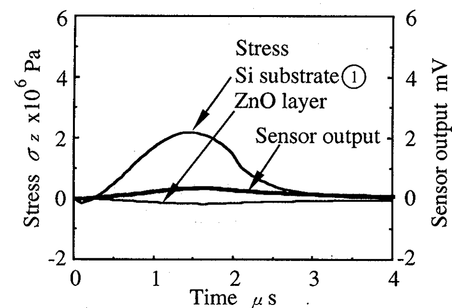

Fig. 15 Simulation of stress and sensor output of the thin-film piezoelectric AE sensor (without backing material)
Simulation conditions
input force: Fig. 11; sensor size: 0.1 mm×0.1 mm; thickness: Si substrate 0.38 mm, ZnO layer 0.002 mm; C_p=0.365 pF; C_e=60 pF; stress calculation: by DYNA 3 D

4.2 Effect of the backing material of the thin-film sensor

To examine the effect of the backing material of the thin-film sensor, we simulated the stress of the piezoelectric layer and the sensor output in the two cases of the sensor model shown in Fig. 10(a) with and without the backing material. The results are shown in Figs. 14 and 15.

In the case of no backing material (Fig. 14), the stress of the piezoelectric layer is small and the sensor output is almost zero. This result corresponds with the sensor output obtained from Eq. (14) with Z_{0b} set to zero. The result shows that the backing material is necessary for increasing sensor sensitivity.

Figure 16 shows the simulated relation between the thickness of the backing material and the maximum output of the sensor. The maximum output of

NII-Electronic Library Service

The Japan Society of Mechanical Engineers

the sensor increases as the thickness of the backing material increases, but it does not change when the thickness of the backing material is more than 0.25 mm.

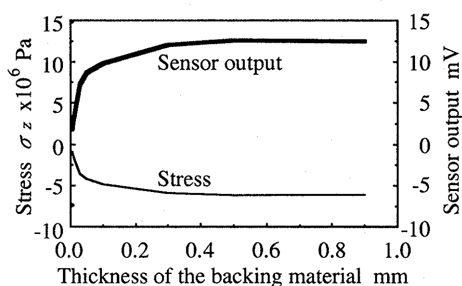

Fig. 16 Simulation of the relation between the thickness of the backing material and the maximum output of the thin-film sessor
Simulation conditions
input force: Fig. 11; sensor size: 0.1 mm×0.1 mm; thickness: Si substrate 0.38 mm, ZnO layer 0.002 mm; C_p=0.365 pF; C_e=60 pF; stress calculation: by DYNA 3 D

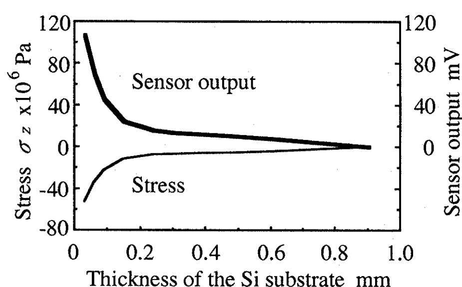

Fig. 17 Simulation of the relation between the thickness of the Si substrate and the maximum output of the thin-film senssor
Simulation conditions
input force: Fig. 11; sensor size: 0.1 mm×0.1 mm; thickness: ZnO layer 0.002 mm, backing material 0.5 mm; C_p=0.365 pF; C_e=60 pF; stress calculation: by DYNA 3 D

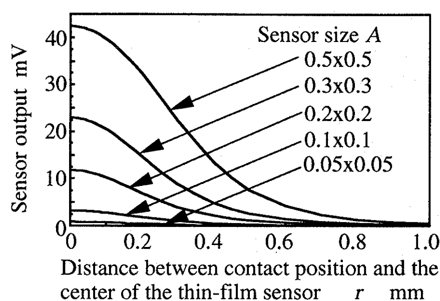

Fig. 18 Simulation of the relation between the contact force and the sensor output
Simulation conditions
thickness: Si substrate 0.38 mm, ZnO layer 0.002 mm; F=1 N; C_p: from Eq.(12); C_e=60 pF; stress calculation: by Eq.(20)

We examined the effect of the backing material on preventing AE waves from reflecting off on the back of the sensor. We checked the stress of the piezoelectric layer and the neighboring Si substrate layer ① and the backing material layer ② in Fig. 10(a).

In Fig. 14, the stress curves of layers ① and ② and the piezoelectric layer are similar to the time function curve of the input force in Fig. 11, and the stress of those three layers are all compressive. Therefore, reflection of AE waves on the boundary surfaces between different materials is thought to be negligible when the sensor has the backing material.

In contrast, in Fig. 15, the stress in the layer ① is compressive and the stress in the piezoelectric layer is tensile. This means that AE waves reflect on the surface between the Si substrate and the piezoelectric layer. This may be the reason why the output of the sensor without backing material is almost zero in Fig. 16.

4.3 Thickness of the Si substrate and output of the sensor

Figure 17 shows the simulated relation between the thickness of the Si substrate and the maximum output of the sensor. The maximum sensor output is large when the Si substrate is thin. Therefore, it is necessary to use a thin Si substrate to obtain high sensitivity of the sensor.

4.4 Distance between the contact force and the sensor and sensor output

We examined the relation between the distance between the contact force and the sensor and output of the sensor. We defined the sensor position as the z-r coordinate shown in Fig. 9 and the area of the sensor element as A. In Fig. 9, z corresponds to the thickness of the Si substrate. We defined z as constant at 0.38 mm in the simulation, because the relation between z and the output of the sensor was already mentioned in section 4.3. We examined the relation between the distance r and sensor output with the sensor area A as a parameter. The stress of the piezoelectric layer was calculated using Eq.(20).

Figure 18 shows the result of the simulation. We can see that the maximum output of the sensor decreases as the distance r increases and when r is larger than 0.8 mm, a sensor with A less than 0.5 mm ×0.5 mm cannot detect AE waves. The maximum output of the sensor is large when A is large and when r is less than 0.6 mm.

We examined the relation between the distance r and sensor output using a sensor fabricated in a slider. In this simulation, we assumed that the four sensor elements of 0.1 mm×0.1 mm were fabricated at the

NII-Electronic Library Service

The Japan Society of Mechanical Engineers

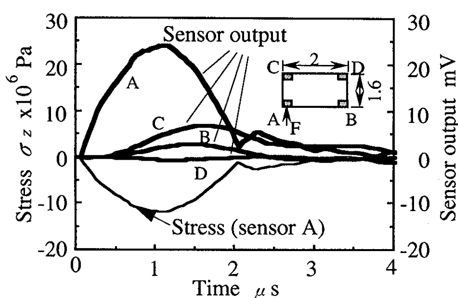

Fig. 19 Simulation of stress and output of the thin-film sensors on the 2-mm-long slider
Simulation conditions: same as Fig. 14

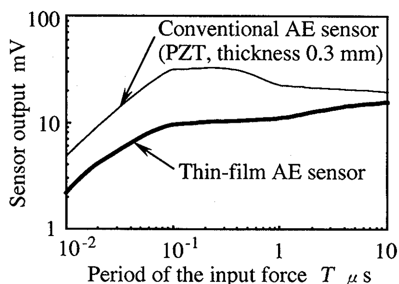

Fig. 20 Simulation of the relation between the sensor output and the duration of the input force
Simulation conditions
input force: Fig. 11; stress calculation: by DYNA3D
Thin-film AE sensor: same as Fig. 14;
Conventional AE sensor size: 0.1 mm×0.1 mm; thickness: slider (Al_2O_3·TiC) 0.38 mm, piezoelectric material (PZT) 0.3 mm; C_p=0.250 pF; C_e=60 pF

four corners of a 2-mm-long slider (50% slider). Figure 19 shows the results of the simulation. Sensor output is large for the sensor in which the distance r is small. The output of the sensor D is almost zero and it shows that the limit of r when the sensor can detect AE waves is about 2.5 mm. Therefore, it is necessary to consider the distance r and the sensor area when designing the sensor.

4.5 Duration of the contact force and sensor output

We examined the bandwidth of the sensor by simulating the relation between the duration of the input force and sensor output. In this simulation, we changed the duration T of the input force in Fig. 11. Figure 20 shows the result of the simulation.

We can see that the sensor output curves of the thin-film sensor and the conventional sensor are similar and that both have a flat section in the region of $T>0.1$ μs. However, at $T<0.1$ μs, the output of both sensors decrease. It is necessary to examine the cause of this in order to increase the bandwidth of the thin-film sensor.

We checked the natural frequencies in the thickness direction of the layers of the sensor slider. In the thin-film sensor, the natural frequency of the piezoelectric layer is quite high but that of the Si substrate is 0.09 μs. Since AE waves propagate from the Si substrate to the thin-film sensor, when the duration of the input force is less than the natural period of the Si substrate, stress caused in the piezoelectric layer becomes small. This may be why the output of the thin-film sensor decreases at $T<0.1$ μs.

In the conventional sensor, the natural periods of the slider (Al_2O_3·TiC) and the piezoelectric material (PZT) are, respectively, 0.06 μs and 0.13 μs. Similarly, when the duration of the input force is less than the natural period of the piezoelectric material, the stress caused in the piezoelectric material is small, and this is the cause of the decrease of the sensor output.

The minimum duration of contact force which the thin-film sensor can detect is about 0.01 μs. It may be possible to increase the sensor bandwidth by using a thinner Si substrate.

5. Summary

We developed a simulation method for examining output characteristics of the thin-film piezoelectric AE sensor to detect the contact between the slider and the disk surface. We confirmed its validity by comparing the result of the simulation with that of the sensor output test. We obtained the following sensor output characteristics from the simulations.

(1) The output of the thin-film sensor (sensor size: 0.1 mm×0.1 mm) per unit input force (1 N) is 12.6 mV/N. This is about half of that of the conventional PZT sensor with the same size (thickness: 0.5 mm).

(2) The effect of the backing material is to prevent AE waves from reflecting off the boundary surface between different materials (it makes the S/N ratio of the sensor high).

(3) The output of the thin-film sensor is negligibly influenced by the thickness of the piezoelectric layer and the backing material. The most important factor in making the sensor sensitivity high is the thickness of the Si substrate.

(4) The minimum duration of the contact force which the thin-film sensor can detect is about 0.01 μs, depending on the natural period of the sensor substrate in the thickness direction.

References

(1) Burger, G. J., Piezoelectric Impact Force Sensor Array for Tribological Research on Rigid Disk Storage Media, Proc. IEEE Micro Electro Mechanical Systems, Workshop, Amsterdam, the

NII-Electronic Library Service

The Japan Society of Mechanical Engineers

Netherlands, Jan. 29-Feb. 2, (1995), p. 294.
(2) Imai, S., A Thin-Film Piezoelectric Impact Sensor Array on a Si Slider for Measuring Head-Disk Interaction, IEEE Transactions on Magnetics, Vol. 31, No. 6, (1995), p. 3009.
(3) Wickert, J.A., Towards a Micromachined Dual Slider and Suspension Assembly for Contact Recording, ASME, Trib. Vol. 3, Concept of Contact Recording, (1992), p. 27.
(4) Auld, B.A., Acoustic Fields and Waves in Solid, (1990), p. 324, Kreiger Publishing Company.
(5) Kawabata, S., Engineering of Ultrasonic Wave, (1988), p. 18, 61, Institute of Industry Research.
(6) Lange, Y.V., Impact Excitation of Vibrations in the Acoustic Spectral Inspection Method, (1979), p. 677, Plenum Publishing Corp..
(7) Timoshenko S.P. and Gooddier, J.N., Theory of Elasticity, (1934), p. 413, McGraw-Hill Book.

NII-Electronic Library Service